

Frequency Conversion Cascade by Crossing Multiple Space and Time Interfaces

Benjamin Apffel¹ and Emmanuel Fort^{1*}

Institut Langevin, ESPCI Paris, PSL University, CNRS, 1 rue Jussieu, 75005 Paris, France

 (Received 27 July 2021; accepted 14 January 2022; published 11 February 2022)

Time varying media recently emerged as promising candidates to fulfill the dream of controlling the wave frequency without nonlinear effects. However, frequency conversion remains limited by the dynamics of the variations of the propagation properties. Here we propose a new concept of space-time cascade to achieve arbitrary large frequency shifts by iterated elementary transformation steps. These steps use an intermediate medium in which wave packets enter and exit through noncommutative space and time interfaces. This concept avoids high frequency or subwavelength demanding metamaterials. Upward and downward frequency conversions are performed. The transmitted energy yield is given by the frequency ratio, regardless of impedance mismatch. We implement this concept with water waves controlled by electrostriction and achieve frequency conversion over 4 octaves.

DOI: 10.1103/PhysRevLett.128.064501

Spatial control of wave propagation has hardly any limits, while time manipulation remains very challenging. Frequency conversion is an essential component of spectral processing upon which much fundamental research [1–4] and countless industrial applications [5–7] are based. It is traditionally performed using nonlinear processes that are amplitude dependent and requires high power signals. Time-varying media have recently opened exciting perspectives for linear frequency conversion based on wave speed variations [8,9]. This relies on the considerable theoretical developments [10,11] and technological achievements in metamaterials, pervading all types of waves such as electromagnetics [12–19], acoustics [20], elastic [21,22], or hydrodynamics [23,24]. However, large frequency conversions are still challenging as the achievable changes in the medium properties are limited.

Here, we introduce the concept of a “space-time cascade” to perform arbitrary large frequency conversions and circumvent the previous limitations. It consists in iterating arbitrarily small transformation steps, consisting of a temporal and a spatial interface. We implement experimentally this concept with water waves and achieve a frequency conversion cascade over 4 octaves.

Comprehensive wave control involves the ability to change the direction and frequency of a wave, i.e., to move the characteristics of the wave from one point (\mathbf{k}_1, ω_1) to another arbitrary point $(\mathbf{k}'_1, \omega'_1)$ on the dispersion cone. To perform such a shift, a common technique is to introduce a second propagating medium 2 with different properties from the original medium 1. In (\mathbf{k}, ω) Fourier space, these two media are represented as two distinct cones as shown in Fig. 1(a). The general idea of space-time cascade is to iterate small steps between the two media in order to achieve arbitrary transformations by successive projections.

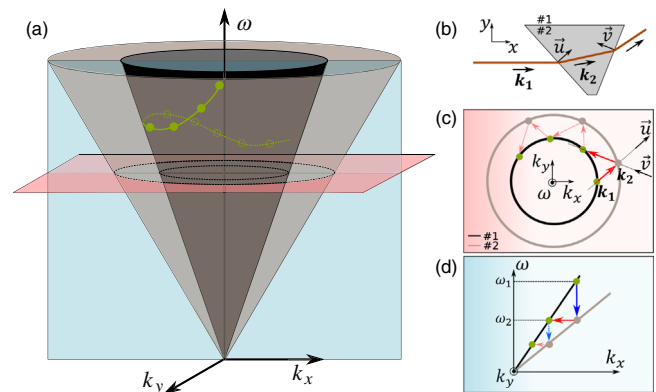


FIG. 1. Principle of wave manipulation by iterative space-time interface crossing between two media. (a) In the (\mathbf{k}, ω) Fourier space, each isotropic medium is represented by a cone given by its dispersion relation. A wave packet in a given medium can be represented as a point on the associated cone. Changing the direction or the frequency of the wave packet can be seen as the displacement (green line) of the point on the cone. (b) Example of a transformation in the horizontal plane (with fixed frequency) for a beam deviated by a prism and (c) the associated transformation in the Fourier space. The initial plane wave (\mathbf{k}_1, ω_1) is deviated by projection of the wave vector in the prism medium (\mathbf{k}_2, ω_1) along the interface normal direction $\mathbf{u} \propto \mathbf{k}_2 - \mathbf{k}_1$ (red arrows) as it enters the prism and is projected again along another direction as it comes back in to the original media. Elementary horizontal transformation (solid line arrows) composed of two space interface crossings with different directions can be iterated to achieve arbitrary wave bending (dashed arrows). (d) For a time interface, the projection is in a vertical plane with $\mathbf{k}_2 = \mathbf{k}_1$ and $\omega_2 \neq \omega_1$ (blue arrows). The iteration of an elementary vertical frequency conversion transformation (solid arrows) composed of a time interface projection followed by a horizontal space interface projection generates arbitrary frequency conversion (dashed arrows). The reflected waves have been omitted for clarity.

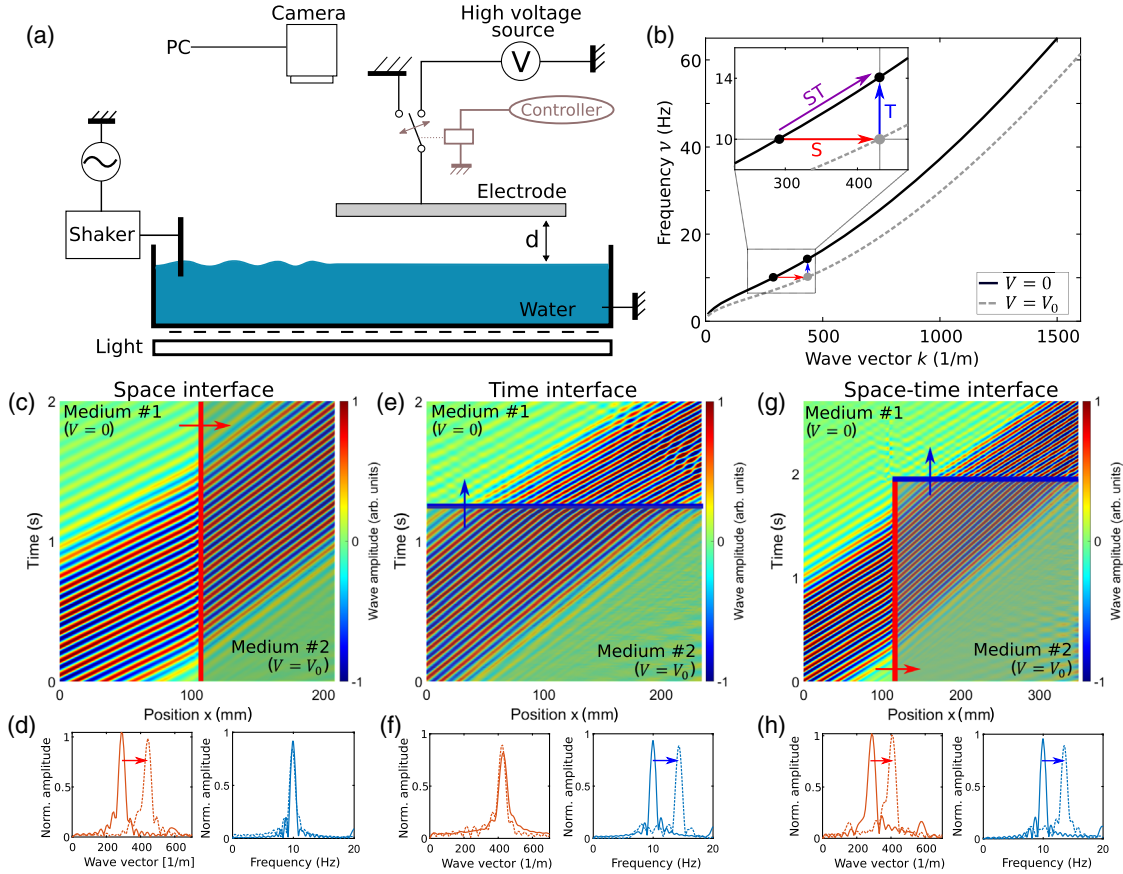


FIG. 2. Experimental implementation of elementary space-time transformation step. (a) Schematic of the experimental setup. The shaker produces a plane water wave packet. The transparent electrode changes medium 1 into 2 by electrostriction with controllable high voltage switches. The wave field is measured by a camera from the deformation of a checkerboard pattern placed under the container [27,28]. (b) Water waves dispersion curves of media 1 with no voltage and 2 with $V_0 = 8.0$ kV and $d = 6$ mm. Example of an elementary frequency up-conversion transformation step composed of successive space projection $S_{1 \rightarrow 2}$ and time projection $T_{2 \rightarrow 1}$ for an initial wave at $\nu = 10$ Hz. Normalized kymographs of a wave packet centered at $\nu = 10$ Hz crossing (c), a space interface $S_{1 \rightarrow 2}$, (e), a time interface $T_{2 \rightarrow 1}$ and (g), the elementary transformation step $T_{2 \rightarrow 1} S_{1 \rightarrow 2}$ [27]. (d), (f), and (h) Normalized k spectra and ν spectra taken before and after the interface crossings, measured from (c), (e), and (g), respectively.

Let us first consider the special case of pure spatial iterations in space, as sketched in Fig. 1(b). To change the direction of a wave packet propagating in a medium 1, it is possible (though a bit artificial) to proceed by successive small changes of direction by using a prism made of medium 2. The wave packet is going through two successive interfaces with different orientations that change the final direction of the wave packet while its frequency remains unchanged. Medium 2 acts as an intermediate medium and at the end, the global change of direction results from the noncommutativity of the two interface crossings. In Fourier space, the initial wave packet can be represented with good approximation by a point with coordinates (\mathbf{k}_1, ω_1) lying on the dispersion cone associated to the propagating media as shown Fig. 1(c). When the wave packet crosses the first prism interface of normal \mathbf{u} , the initial point (\mathbf{k}_1, ω_1) experiences a projection $S_{1 \rightarrow 2}$ and ends up at coordinate $(\mathbf{k}'_1, \omega_1)$ on the dispersion cone associated to the prism. As the frequency is not affected by

the interface, the projection occurs in the horizontal plane associated to constant ω slicing the two cones as shown in Figs. 1(a) and 1(c). The projection direction of $S_{1 \rightarrow 2}$ is given by $\mathbf{k}'_1 - \mathbf{k}_1 \propto \mathbf{u}$ giving a simple geometrical construction of the projection. In the same manner, the wave packet will experience a second horizontal projection $S'_{2 \rightarrow 1}$ with direction given by the normal to the second interface to exit the prism. As $S_{1 \rightarrow 2}$ and $S'_{2 \rightarrow 1}$ do not commute, the wave comes back on the first cone with different coordinates compared to its initial position. Even though the transformations allowed by one prism are quite limited, iterating this process allows us to implement arbitrary rotation on the dispersion cone in the horizontal plane. The concept of space-time cascade is based on the same idea to move vertically on the dispersion cone using an iteration of elementary steps composed of a time and a space interface [see Fig. 1(d)]. Projections associated with time interfaces, $T_{1 \rightarrow 2}$, are obtained by a temporal change of the propagation properties from medium 1 to 2 [8,17,19].

In this case, momentum is conserved ($k_2 = k_1$) while the frequency changes $\omega_2 \neq \omega_1$ [Fig. 1(d)], leading to a vertical projection between the dispersion curves of the two media. If one comes back in medium 1 with a spatial interface $S_{2 \rightarrow 1}$ corresponding to a horizontal projection, both the frequency and the wave vector are changed through the global transformation $S_{2 \rightarrow 1} T_{1 \rightarrow 2}$ [25].

In practice, the dispersion cones of the two media are very close to each other due to the difficulty of significantly varying the propagation properties of a medium. Step transformations therefore induce very limited frequency shifts $\Delta\nu$. However, these small shifts can be added by iteration [Fig. 1(d)] allowing arbitrarily large transformations between two media with arbitrarily close properties. Any trajectory on the dispersion cone characterizing wave bending and frequency conversion can be implemented using this concept [Fig. 1(d)]. Frequency conversions can be achieved by cascading elementary vertical steps to form a staircaselike transformation with *a priori* no limitation. A simple permutation of space and time interfaces can change a blueshift into a redshift, going up or down the transformation staircase. The commutated product, changing $T_{2 \rightarrow 1} S_{1 \rightarrow 2}$ to $S_{2 \rightarrow 1} T_{1 \rightarrow 2}$, corresponds to the time-reversed transformation. Since the transformations are linear, the previous considerations can easily be extended to wave packets with arbitrary frequency spectra.

We implemented this concept with electrostriction-controlled water waves. When a flat electrode is mounted above the grounded conductive water surface, the applied electric field exerts an attractive force on the liquid surface that changes the velocity of the water wave [26]. This creates well-controlled space and time varying properties. Figure 2(a) shows the experimental setup consisting of a container filled with tap water [27]. Transparent FTO electrodes are suspended horizontally at a distance d above the water. The electric potential V can be tuned in the range of 0 to 10 kV using electrical switches. Plane waves are produced by a shaker exciting horizontally a paddle. The wave field is measured from top-view images using the deformation of a checkerboard pattern placed below [28]. For a given wave number k , the voltage-dependent refractive index $n(k, V)$ satisfies

$$\begin{aligned} n(k, V) &= [1 - \chi_0(k)V^2]^{-\frac{1}{2}} \quad \text{with} \\ \chi_0(k) &= \epsilon / [\rho c^2(k)d^2 \tanh(kd)]. \end{aligned} \quad (1)$$

$c(k)$ is the wave velocity given by the gravity-capillary dispersion relation at $V = 0$, ϵ is the dielectric permittivity of air, and ρ is the density of the liquid [26]. Figure 2(b) shows the dispersion relation (1) for $V = 0$ kV (medium 1) and for $V = V_0$ (medium 2) as well as the frequency up-conversion transformation step consisting of a space interface $S_{1 \rightarrow 2}$ followed by a time interface $T_{2 \rightarrow 1}$. The space interface is located at the edge of the electrode where the refractive index varies typically over a width $\sim d$.

Figure 2(c) shows the experimental normalized kymograph of a wave packet crossing the interface $S_{1 \rightarrow 2}$ as it enters under the electrode set at V_0 to produce a change of refractive index $\Delta n \approx 0.5$ [27]. The wave vector is shifted by $\Delta k \approx +200 \text{ m}^{-1}$ while its frequency spectrum remains unchanged [Fig. 2(d)]. The wave packet propagating under an electrode can also cross a time interface $T_{2 \rightarrow 1}$ when the voltage V_0 is switched off, resulting in a sudden change $\Delta n \approx -0.5$ [27]. The frequency spectrum is blueshifted by $\Delta\nu \approx +4 \text{ Hz}$ while the k -spectrum remains unchanged [Fig. 2(f)]. The complete elementary transformation step consisting of a succession of interfaces $S_{1 \rightarrow 2}$ and $T_{2 \rightarrow 1}$ [Fig. 2(g)] shifts both the frequency and the wave vector [Fig. 2(h)] to satisfy the dispersion relation of medium 1. The kymographs show transformation steps as space-time tessellation. Medium 2 appears as square patterns which size depends on the space-time extension of the wave packet [27].

The experimental setup can be modified to perform frequency conversion cascades [Fig. 3(a)]. The wave packet undergoes multiple transformation steps $T_{2 \rightarrow 1} S_{1 \rightarrow 2}$ as it propagates under successive electrodes. The wavelength λ of the wave packet decreases after each step [Fig. 3(b)] compared to a free propagating reference, Fig. 3(c)]. These contractions are associated to the blueshift in frequency satisfying $\nu = (c/\lambda)$ [Fig. 2(b)] [27]. The frequency spectrum is shifted by $\Delta\nu \approx 2 \text{ Hz}$ at each step [Fig. 3(d)]. The opposite redshift cascade can also be achieved by the time

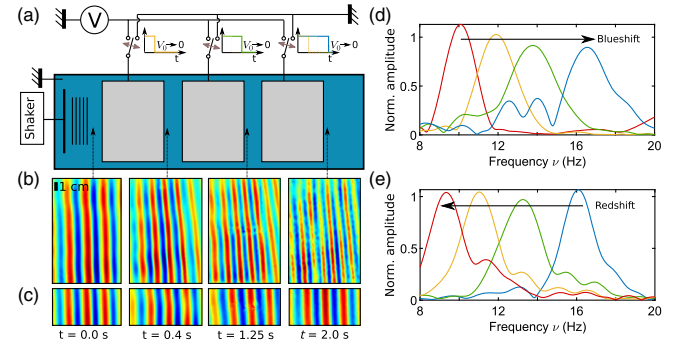


FIG. 3. Experiment of the frequency conversion cascade. (a) Schematic of the space-time cascade experimental setup (top view) with 3 electrodes controlled by independent electrical switches. The plane wave packet with $\nu \approx 10 \text{ Hz}$ undergoes 3 successive elementary transformation steps $T_{2 \rightarrow 1} S_{1 \rightarrow 2}$ as it passes under each electrode initially set at V_0 and switched off synchronized with the wave propagation (see insets). (b) Snapshots of the initial wave packet ($t = 0.0 \text{ s}$) and of the successive frequency shifts after each transformation step at $t = 0.4, 1.25, \text{ and } 2.0 \text{ s}$ [27]. Color encodes wave amplitude in arb. units. (c) Snapshots of the same propagating wave packet taken in the absence of voltage (reference). (d) Frequency spectra of the snapshots (b) showing a blueshift $\Delta\nu \approx 2 \text{ Hz}$ for each transformation step. (e) Frequency spectra associated with the time reversed process for an initial wave packet of $\nu \approx 16 \text{ Hz}$ redshifted by successive elementary transformation steps $S_{2 \rightarrow 1} T_{1 \rightarrow 2}$ [27].

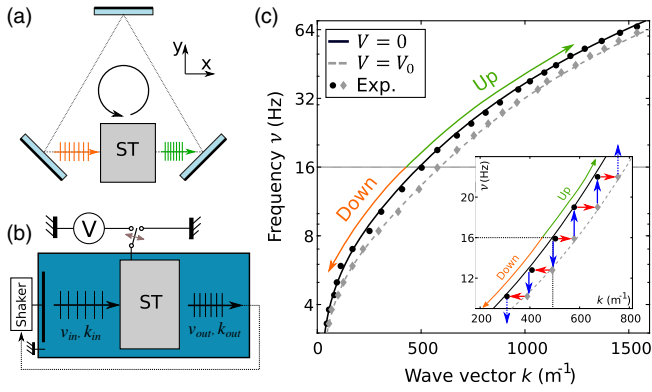


FIG. 4. Frequency conversion cascade confined within a cavity. (a) Example of a cavity with a triangle geometry to perform multiple passes under the same electrode. The circulating wave packet is limited to the size of active medium (ST) with no links to the cavity modes. (b) Experimental implementation in a modified Fabry-Pérot cavity with an amplification loop to compensate for the poor reflection efficiency of water waves. (c) Up and down frequency conversion cascades and dispersion curves from Eq. (1) in semilogarithmic scale for an initial wave packet at $\nu = 16$ Hz. (inset: close-up).

reversed operation with successive time-flipped steps $S_{2 \rightarrow 1} T_{1 \rightarrow 2}$ [Fig. 3(e)] [27].

Other geometries are more suitable when the number of transformation steps increases. Cavities, such as a unidirectional triangular geometry [Fig. 4(a)] or a Fabry-Pérot cavity, allow a single active medium to perform all the transformation steps. The time interface is synchronized when the circulating wave packet is in the active medium. Since the extension of the wave packet is limited, it is completely independent of the cavity modes in contrast to time-varying resonator experiments [9,12,13,30]. Because of the limited efficiency of water wave reflection, an amplification loop must be used to send the wave packet back into the active medium [Fig. 4(b)]. With damping compensation, a cascade of up and down frequency conversion can be achieved over a range of more than 4 octaves with 23 elementary steps [Fig. 4(c)].

As in most time-varying experiments, electrostriction-driven interfaces have an impedance mismatch creating reflected waves. These small amplitude waves can be further reduced by antireflection coating [17] or by using smoother interfaces [29]. In the space-time cascade, the duration of time interfaces is limited only by the residence time of the wave packet in the active medium. This is an asset for implementation with other types of waves such as in optics.

We now focus on the role of the impedance mismatch on the wave amplitude transmission yield through an elementary transformation step. Impedance mismatch results in the creation of the reflected wave packet at the (either space or time) interface. However, energy and momentum conservations differ depending on the type of interface. In the case of spatial interface, the energy

flux of an incident wave packet is conserved but splits into the transmitted wave packet and the reflected one. Hence, the transmitted energy flux after the interface is always lower than the incident one without impedance matching. Temporal interfaces on the other hand do not conserve energy flux as they break the time translational invariance. The sum of energy flux of the transmitted and reflected wave packets is not equal to the energy of the incident one and can be smaller or larger. For an elementary step transformation composed of sharp space and time interfaces, the total transmitted energy of the wave packet normalized by the incident one satisfies the simple relation $\Gamma = \omega'/\omega$, independent of the order of the interfaces (see Supplemental Material) [8,27]. In terms of momentum, spatial interfaces do not conserve momentum. The sum of the reflected and transmitted momentum does not equal the incoming one. For time interface, the momentum is conserved due to the spatial translation symmetry and the sum of the sign-opposed momentum of the reflected and transmitted wave packet equals that of the incident momentum. For an elementary step transformation, the total transmitted momentum of the wave packet normalized by the incident one also satisfies $\Gamma = \omega'/\omega$. The total transmitted energy is thus independent of the impedance mismatch. However, the later induces a reflected wave at the space interface and the production of two counter-propagating additional waves at the time interface. The loss in transmission at the space interface is related to the gain at the time interface resulting in an impedance independent result (see Supplemental Material [27]).

The ratio $\Gamma = \omega'/\omega$ for an elementary step naturally leads to an interpretation in terms of number of photons with energy $\hbar\omega$ before the conversion and $\hbar\omega'$ after. Far from interfaces, the number of incoming photons $N \propto E/\omega$ is equal to the number of outgoing transmitted photons $N' \propto E'/\omega'$. The loss of photons by reflection due to the spatial interface is compensated by the gain at the temporal interface. These results are valid provided that both space and time interfaces are sharp. Breaking this symmetry by smoothing one interface could enable us to engineer the output yield and amplify or damp the transmitted wave packet.

The space-time cascade requires us to texture the propagating medium in space and time with a characteristic size given by the wave packet. It thus differs from the widespread regime of parametric excitation for which the modulation of the medium property is typically of the order of the wave frequency. Unlike parametric excitation, energy gain or loss can occur even in the case of impedance matching as the intrinsic properties of the wave packet are modified undergoing a series of noncommutable space-time transformation steps.

Interestingly, a gain process in impedance-matched modulated medium has recently been described for waves propagating in luminal materials, in which the index

modulation moves at or close to the velocity of light. A redistribution of the lines of force in space can lead to net energy gain of the propagating wave [31]. Electrostriction offers a versatile spatiotemporal control that would allow us to experimentally implement this original amplification mechanism in a simple and controllable way, as well as other more complex spatiotemporal modulations.

The authors would like to thank Mathias Fink and Antonin Eddi for fruitful discussions and Samuel Hidalgo for his precious help in setting the electric part of the experimental setup. The authors thank the support of AXA research fund and the French National Research Agency LABEX WIFI (ANR-10-LABX-24).

*Corresponding author.
emmanuel.fort@espci.fr

- [1] J. T. Mendonça, G. Brodin, and M. Marklund, Vacuum effects in a vibrating cavity: Time refraction, dynamical Casimir effect, and effective Unruh acceleration, *Phys. Lett. A* **372**, 5621 (2008).
- [2] N. Westerberg, S. Cacciatori, F. Belgiorno, F. D. Piazza, and D. Faccio, Experimental quantum cosmology in time-dependent optical media, *New J. Phys.* **16**, 075003 (2014).
- [3] N. Engheta, Pursuing near-Zero response, *Science* **340**, 286 (2013).
- [4] G. W. Milton and O. Mattei, Field patterns: A new mathematical object, *Proc. R. Soc. A* **473**, 20160819 (2017).
- [5] N. Matsuda, Deterministic reshaping of single-photon spectra using cross-phase modulation, *Sci. Adv.* **2**, e1501223 (2016).
- [6] D. Ramaccia, A. Alù, A. Toscano, and F. Bilotti, Temporal multilayer structures for designing higher-order transfer functions using time-varying metamaterials, *Appl. Phys. Lett.* **118**, 101901 (2021).
- [7] H. Nassar, B. Yousefzadeh, R. Fleury, M. Ruzzene, A. Alù, C. Daraio, A. N. Norris, G. Huang, and M. R. Haberman, Nonreciprocity in acoustic and elastic materials, *Nat. Rev. Mater.* **5**, 667 (2020).
- [8] F. Morgenthaler, Velocity modulation of electromagnetic waves, *IRE Trans. Microwave Theory Tech.* **6**, 167 (1958).
- [9] M. Notomi and S. Mitsugi, Wavelength conversion via dynamic refractive index tuning of a cavity, *Phys. Rev. A* **73**, 051803(R) (2006).
- [10] Y. Xiao, G. P. Agrawal, and D. N. Maywar, Spectral and temporal changes of optical pulses propagating through time-varying linear media, *Opt. Lett.* **36**, 505 (2011).
- [11] P. A. Huidobro, E. Galiffi, S. Guenneau, R. V. Craster, and J. B. Pendry, Fresnel drag in space-time-modulated metamaterials, *Proc. Natl. Acad. Sci. U.S.A.* **116**, 24943 (2019).
- [12] T. Tanabe, M. Notomi, H. Taniyama, and E. Kuramochi, Dynamic Release of Trapped Light from an Ultrahigh-Q Nanocavity via Adiabatic Frequency Tuning, *Phys. Rev. Lett.* **102**, 043907 (2009).
- [13] S. Preble, Q. Xu, and M. Lipson, Changing the color of light in a silicon resonator, *Nat. Photonics* **1**, 293 (2007).
- [14] A. M. Shaltout, K. G. Lagoudakis, J. van de Groep, S. J. Kim, J. Vučković, V. M. Shalaev, and M. L. Brongersma, Spatiotemporal light control with frequency-gradient metasurfaces, *Science* **365**, 374 (2019).
- [15] V. Bruno, S. Vezzoli, C. DeVault, E. Carnemolla, M. Ferrera, A. Boltasseva, V. M. Shalaev, D. Faccio, and M. Clerici, Broad frequency shift of parametric processes in Epsilon-near-Zero time-varying media, *Appl. Sci.* **10**, 4 (2020).
- [16] Y. Zhou, M. Z. Alam, M. Karimi, J. Upham, O. Reshef, C. Liu, A. E. Willner, and R. W. Boyd, Broadband frequency translation through time refraction in an Epsilon-near-Zero material, *Nat. Commun.* **11**, 2180 (2020).
- [17] V. Pacheco-Peña and N. Engheta, Antireflection temporal coatings, *Optica* **7**, 323 (2020).
- [18] A. Silva, F. Monticone, G. Castaldi, V. Galdi, A. Alù, and N. Engheta, Performing mathematical operations with metamaterials, *Science* **343**, 160 (2014).
- [19] C. Caloz and Z.-L. Deck-Léger, Spacetime metamaterials—Part I: General concepts, *IEEE Trans. Antennas Propag.* **68**, 1569 (2020).
- [20] R. Fleury, A. B. Khanikaev, and A. Alù, Floquet topological insulators for sound, *Nat. Commun.* **7**, 11744 (2016).
- [21] G. Trainiti, Y. Xia, J. Marconi, G. Cazzulani, A. Erturk, and M. Ruzzene, Time-Periodic Stiffness Modulation in Elastic Metamaterials for Selective Wave Filtering: Theory and Experiment, *Phys. Rev. Lett.* **122**, 124301 (2019).
- [22] A. Darabi, X. Ni, M. Leamy, and A. Alù, Reconfigurable floquet elastodynamic topological insulator based on synthetic angular momentum bias, *Sci. Adv.* **6**, eaba8656 (2020).
- [23] V. Bacot, M. Labousse, A. Eddi, M. Fink, and E. Fort, Time reversal and holography with spacetime transformations, *Nat. Phys.* **12**, 972 (2016).
- [24] V. Bacot, G. Durey, A. Eddi, M. Fink, and E. Fort, Phase-conjugate mirror for water waves driven by the faraday instability, *Publ. Natl. Acad. Sci. U.S.A.* **116**, 8809 (2019).
- [25] F. Biancalana, A. Amann, A. V. Uskov, and E. P. O'Reilly, Dynamics of light propagation in spatiotemporal dielectric structures, *Phys. Rev. E* **75**, 046607 (2007).
- [26] C.-S. Yih, Stability of a horizontal fluid interface in a periodic vertical electric field, *Phys. Fluids* **11**, 1447 (1968).
- [27] See Supplemental Material at <http://link.aps.org/supplemental/10.1103/PhysRevLett.128.064501> for details and videos 1–3.
- [28] S. Wildeman, Real-time quantitative schlieren imaging by fast fourier demodulation of a checkered backdrop, *Exp. Fluids* **59**, 97 (2018).
- [29] A. G. Hayrapetyan, J. B. Götze, K. K. Grigoryan, S. Fritzsche, and R. G. Petrosyan, Electromagnetic wave propagation in spatially homogeneous yet smoothly time-varying dielectric media, *J. Quant. Spectrosc. Radiat. Transfer* **178**, 158 (2016).
- [30] P. Dong, S. F. Preble, J. T. Robinson, S. Manipatruni, and M. Lipson, Inducing Photonic Transitions between Discrete Modes in a Silicon Optical Microcavity, *Phys. Rev. Lett.* **100**, 033904 (2008).
- [31] J. B. Pendry, E. Galiffi, and P. A. Huidobro, Gain in time-dependent media—a new mechanism, *J. Opt. Soc. Am. B* **38**, 3360 (2021).